Hybrid Generators-based AC Microgrid Performance Assessment in Island Mode

Walid Issa [1*], Suleiman Sharkh [2], Mohammad Abusara [3]

[1] Electrical Engineering Department, Sheffield Hallam University, Pond Street S1 1WB, Sheffield, UK

[2] Electro-Mechanical Engineering Research Group, University of Southampton, Southampton, SO17 1BJ , UK

[3] Renewable Energy Research Group, University of Exeter, Penryn, TR10 9EF, UK

[*] wissa@outlook.com

Abstract – Achieving an accurate steady-state averaged active power sharing between parallel inverters in islanded AC microgrids could be realized by a traditional droop control. For identical inverters having the same droop gains, it is assumed that the transient average power responses will be similar, and no circulating current will flow between the units. However, different line impedances could influence the instantaneous power significantly and thus circulating power flows among the inverters particularly during sudden disturbances such as load changes. This power, if absorbed by an inverter, will lead the DC link voltage to rise abruptly and trip the inverter, thus, degrading the performance of the whole microgrid. The problem becomes worse when hybrid generators are serving as unidirectional power source. This paper assesses the performance of hybrid generators within an islanded microgrid against the mismatch in line impedances. Two schemes to stabilize the microgrid are proposed. In addition, a participation factor analysis is developed to select the most effective controller scheme to bound the DC link voltage and minimize the circulating power. Simulation and experimental results are presented to verify the analysis and the capability of the proposed controller.

1. Introduction

A microgrid is an energy system composed of loads and distributed energy resources (DER) such as distributed generators (DG) and energy storage systems (ESS) that can operate either in island or grid-connected configuration [1]. Power electronic inverters are used to integrate energy sources such as PV, wind, batteries to form an AC microgrid. Parallel operation improves redundancy, which further improves reliability.

Power sharing between parallel inverters using droop control has been extensively used and reported in the literature because it is easy, simple and inherently responsive when connected in parallel with synchronous generators [2]-[4]. In addition, it only uses local measurements without the need for high speed communications. To maintain good stability margins for the system, the droop control loops have to be designed with lower bandwidth than that of the inner voltage and current regulation loops. This requires using small droop gains and/or using slow power measurement low pass filters [5]-[6]. Droop gains are chosen to give satisfactory transient power response and acceptable steady state deviation in voltage and frequency. It is capable of achieving accurate steady state averaged active power sharing between parallel inverters despite of any mismatch in the inverter's output impedances and line impedances. However, it does not guarantee equitable sharing of transient power. Large mismatch in line impedance results in large differences in transient power circulation between the inverters. This energy can be absorbed by a DC/DC converter if the energy source is a battery, for example, to maintain a regulated DC link voltage. However, in case of unidirectional source as fuel cell or micro-gas turbine, the circulating power can't be absorbed or ceased causing unstable DC link response [7].

Many controllers have been proposed in the literature to improve the averaged transient power responses of paralleled inverters. Guerrero *et al.* [8] introduced power derivative-integral terms into the conventional droop control to improve the dynamic response and to minimize the circulating currents between the paralleled inverters. Avelar *et al.* [6] proposed an extra phase loop to mitigate the transient response peak and to avoid overrating the unit. In [9], a supplementary loop was proposed around the conventional droop control to stabilize the system while using high power angle droop gains. Other auxiliary loops were presented in [10] and [11] with the droop controller to increase the system's damping.

Adaptive droop controllers were also proposed in [12] and [13] to improve the control performance and to provide seamless mode transfer. In [14], an adaptive derivative term was added to the droop controller to decrease current overshoot and improve stability. Piecewise linear droop control was presented in [15] and gain-scheduled decoupling control strategies were proposed in [16]. In [17], a central controller with low bandwidth communication is employed in order to tune the droop parameters properly under different load conditions.

Although the abovementioned studies have focused on improving the transient dynamics of average power control, none has addressed the instantaneous transient power impact on the stability of the parallel inverters. Furthermore, none of these studies considered the effect of mismatched line impedances on microgrid system damping and circulated energy. In our previous study [7], we investigated the impact of circulating power on DC link voltage under unintentional islanding case and a controller was proposed to stabilize the DC link voltage. The findings approved the significance of such studies in improving the operational reliability of the microgrids.

This paper investigates the impact of mismatched line impedances on the performance of parallel inverters supplied by different energy sources and assesses the instantaneous circulating power responses against the stability of the microgrid. A small signal state space model of a microgrid

consisting of three inverters is used to analyse the system. Two controller schemes based on supplementary phase and frequency loops are proposed to maintain the microgrid stability. A participation factor assessment is used to select the most effective controller scheme with the least action to bound the DC link voltage. The proposed controller has been validated by simulation and experimentally.

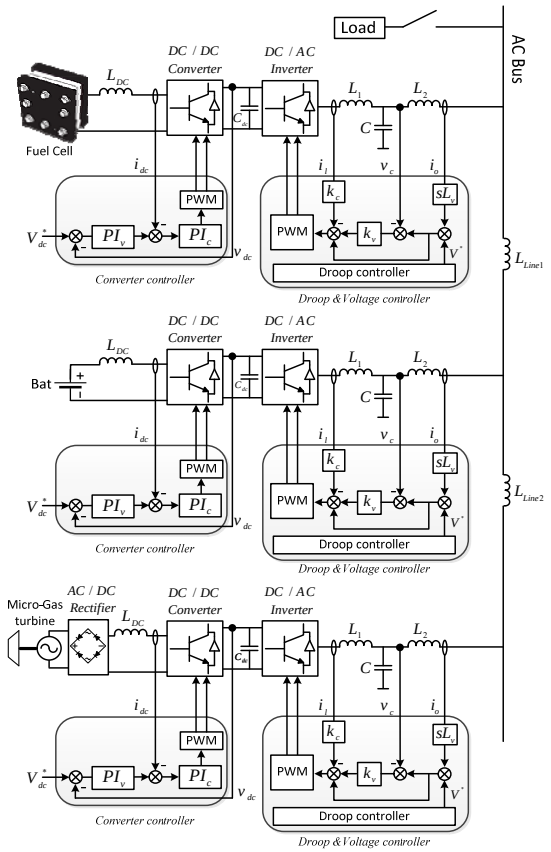

Fig. 1 Microgrid structure under study

2. System Overview

Fig. 1 shows a microgrid system composed of three DG units supplied by different energy sources. Each DG unit has a DC/DC converter and a DC/AC inverter with a DC link capacitor in between. For a battery-based energy source, the DC link voltage is regulated by a bidirectional buck/boost DC/DC converter [18]. For fuel cells and gas micro turbine - based systems unidirectional boost DC/DC converters are used. Typically, in such a system, the gas turbine is taking the role of controlling the AC bus voltage and frequency. However, in our system, it will work as an auxiliary supply and the battery-based system will fulfill the bus control requirements. This supports the carbone emission reduction plans. Furthermore, the battery system can generate and absorb power to and from the AC bus to balance the power flow by the droop control while the auxiliary supply can only generate power. This might be advantageous when the generation is more than the load which gives the chance inherently to charge the battery if possible [19]. Also it is worth mentioning that the DC link voltage of the fuel cell-based unit could be controlled by the inverter side controller or by the DC converter controller [20]-[22]. To maintain the consistency and to simplify the modelling, the DC converter is chosen to regulate the DC link voltage knowing that this might degrade the power efficiency.

Normally, there is no control link between the DC/DC converters and DC/AC inverters. The DC/DC converters regulate the DC link voltage against any disturbances caused by the inverter side. The inverters manage the output power and voltage to satisfy the load demand. In the next sections, the study highlights cases where the DC link voltage can't be controlled because of this isolation between the controllers of the two converters.

In cascaded control systems, and as a rule of thumb, the inner voltage loop must have a bandwidth that is 3-5 times higher than that of the outer power loop to preserve the stability and tracking resolution [14]. The modelling of a microgrid adopting the droop controller is well-established in the literature [7]-[25]. The inner voltage loop is normally neglected in the modelling because its response time is much faster than the outer droop control loop. In addition, the droop control is developed based on the steady-state analysis of power flow. As a result, the dynamics of the power control loop shall be sufficiently slower than the DG voltage tracking dynamics [3]. Therefore, each inverter can be modelled by its Thevenin equivalent circuit as shown in Fig. 2. The equivalent circuit model consists of an ideal voltage source, V_o, and an output impedance; $R_o + j\omega L_o$; which can be calculated as in [26] and [27]. The voltage source will be controlled directly by the droop equations.

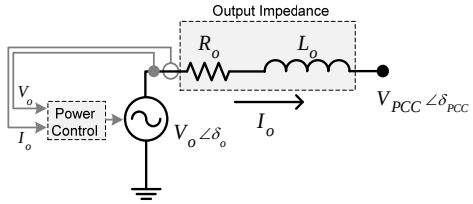

Fig. 2 Thevenin equivalent model of an inverter

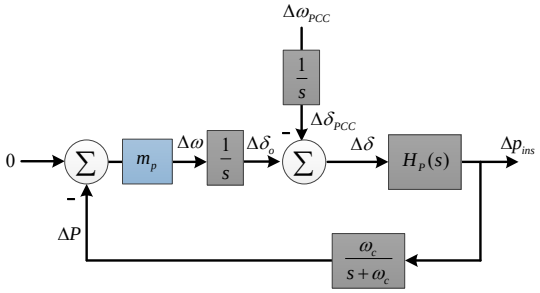

Fig. 3 Small signal model of the droop controller for one inverter

The bus voltage is assumed to be well controlled. Therefore, to simplify the modelling and analysis, the considered load type in this paper is the constant impedance load model. It is a static load model where the power varies with the square of the voltage magnitude. Other load models like constant current and constant power loads can be studied in future works if needed. However, the problem happens in low load, ideally zero, cases as will be explained in the next section. Thus, the type of load is expected to have an insignificant impact on the considered problem.

3. Droop Control Operation

The frequency and voltage droops are described by (1) and (2), respectively as:

$$\omega = \omega_o - m_p P, \quad (1)$$

$$V = V_o - n_q Q, \quad (2)$$

where ω_o , V_o , m_p, and n_q are the nominal frequency, nominal voltage, frequency droop coefficient, and voltage droop coefficient, respectively. P and Q are the average measured output active and reactive powers, respectively.
Average power is obtained from the instantaneous power p_{ins} using a low pass filter as,

$$P = \frac{\omega_c}{s+\omega_c} p_{ins}, \quad (3)$$

where ω_c is the cut-off frequency which is chosen to be much lower than the fundamental frequency to provide good filtration and frequency independence of the dynamics of the inner loops. From Fig. 2, the instantaneous output active power is related to the power angle and given by

$$p_{ins} = \frac{V_o V_{PCC} \sin(\delta_o - \delta_{PCC})}{X_o}, \quad (4)$$

where V_o and V_{PCC} are the output voltages, δ_o and δ_{PCC} are the phase angles of the inverter and PCC nodes, respectively. X_o is the equivalent output reactance of the inverter where R_o is neglected. By perturbing (1) we get

$$\Delta\omega = -m_P \Delta P . \quad (5)$$

By perturbing (4) and assuming constant V_o, V_{PCC} we get,

$$\Delta p_{ins} = H_P \Delta\delta , \quad (6)$$

where $H_p = \frac{V_o V_{PCC} \cos(\delta_{eq})}{X_o}$, $\Delta\delta = \Delta\delta_o - \Delta\delta_{PCC}$, δ_{eq} is the equilibrium point of the phase difference around which the perturbation is performed. From (3), (5) and (6), the small signal model of the droop control loop can be represented by the block diagram of Fig. 3. By ignoring the LPF in Fig. 3, the transfer function that relates the output power ΔP to the bus frequency $\Delta\omega_{PCC}$ is given by

$$\Delta P = \frac{-H_p}{s + m_p H_p} \Delta\omega_{PCC} \quad (7)$$

Two observations can be made from (7). First, the DC gain equals $-1/m_p$ which means that if the inverters have the same m_p, they will all achieve equal steady state active power sharing. However, the transient response is determined by the pole $-m_p H_p$ which depends on both values of m_p and H_p. Consequently, equal m_p gains will not guarantee equal transient power sharing between the inverters unless all H_p are equal, i.e, X_o are equal. The corresponding transient instantaneous power, if negative, causes a rise in the DC link voltage. The second observation is that the dynamic response of the droop controller is significantly affected by X_o, which is determined by the inverter's output impedance and the line impedance between the inverter and the PCC. Thus, each inverter might have different damping depending on its location within the microgrid. It is important to take this into account when determining the droop gain m_p, which is normally chosen to satisfy the steady state condition such as

$$m_p \le \frac{\omega_{\max} - \omega_{\min}}{P_{\max}}, \quad (8)$$

where ω_{max} and ω_{min} are the maximum and minimum allowable values of frequency and P_{max} is the maximum output average active power of the inverter.
In Fig. 3, the frequency at the PCC, $\Delta\omega_{PCC}$, is represented as a disturbance to the droop controller, which is mainly determined by the load. It is important to study the effect of varying loads on the transient power and hence on the stability of the DC link voltage. Unfortunately, the small signal model in Fig. 3 cannot be used for this study because a whole microgrid model needs to be developed in order to determine $\Delta\omega_{PCC}$. A state space small signal model was developed by the authors in a previous work will be used for this study in the next sections.

4. Dynamic Analysis

The microgrid model developed in [23] will be used in this paper to assess the microgrid stability when the load changes abruptly with the existence of significant line impedance mismatch. The model was verified by detailed simulation results and also by experimental results in [24]. The model was established in the rotating DQ frame including the dynamics of the power loops, network, and loads. The state space model has the form of

$$\dot{x} = Ax$$

$$x = \Big[\underbrace{\Delta\omega \quad \Delta\delta \quad \Delta P \quad \Delta Q \quad \Delta v_{dc} \quad \Delta i_{od} \quad \Delta i_{oq}}_{FC} \quad \underbrace{\Delta\omega \quad . \quad . \quad \Delta i_{oq}}_{Batery} \quad \underbrace{\Delta\omega \quad . \quad . \quad \Delta i_{oq}}_{\mu GT} \quad \underbrace{\Delta i_{LineD} \quad \Delta i_{LineQ} \quad . \quad .}_{Distribution\ lines} \quad \underbrace{\Delta i_{LoadD} \quad \Delta i_{LoadQ} \quad . \quad .}_{Loads} \Big]^T \quad (9)$$

where A is the state space matrix.
As was shown in (7), the line impedance alters the locations of the designed eigenvalues and hence the damping. Fig. 4a shows the dominant eigenvalues of the microgrid when the three inverters have $1mH$ output inductance with negligible line impedances (see Fig.) and m_p varies from 5×10^{-5} to 5×10^{-3}. The eigenvalues traces are identical and the inverters will behave similarly. Fig. 4b shows the same traces but with different line inductances: $L_{Line1} = 1mH$ and $L_{Line1} = 2mH$. It is clear that for the same m_p range, the corresponding eigenvalues represent different damping ratios and the poles are shifted from their original locations. This might increase oscillation and overshoot highly. The eigenvalues when $m_p = 3 \times 10^{-3}$ are highlighted in both figures to show that the same droop gain produces different damping ratios of the output power responses. Increasing m_p is desirable for achieving high sharing accuracy but it degrades the stability.
Therefore, during load changes, i.e., full to zero load, the transient responses of paralleled inverters will not be identical even if equal design parameters are chosen. The highly damped inverters will respond slower to the change than the low damped inverter which will approach the steady state faster. If the new steady state values for the active power are close to zero, the power will circulate from the highly damped inverter to the lightly damped ones during the transient. This will charge the DC link capacitor and push the DC voltage to higher values which can trip the system. With the parameters in Table 1 and with the droop gains selected according to (8), a microgrid model was built in Matlab/Simulink. The active power responses and the corresponding DC link voltages are obtained when the load changed suddenly from 100% to 0%. Fig. 5 shows the responses when identical distribution lines are used, $L_{Line1,2} = 0$. The responses are quite identical and the DC link voltages are only slightly affected. In Fig. 6, the power responses are differently damped and some power is imported. If the DC/DC converter is bi-directional as for the battery systems, it will sink the power from the DC link capacitor. However, if the DC/DC converter is unidirectional as in the systems of fuel cell and gas micro-turbines, the DC voltage can't be bounded as shown in Fig. 6b.

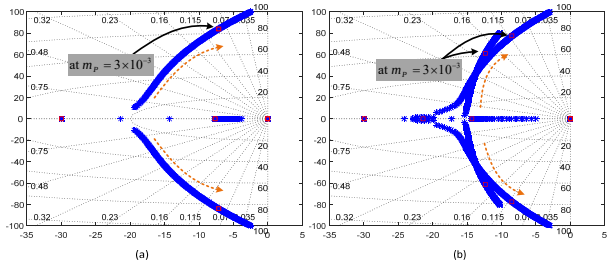

Fig. 4 Dominant system eigenvalues when $0.5 \times 10^{-4} > m_p > 5 \times 10^{-3}$ and lines inductances are (a) neglected (b) $L_{Line1} = 1mH$ *and* $L_{Line1} = 2mH$

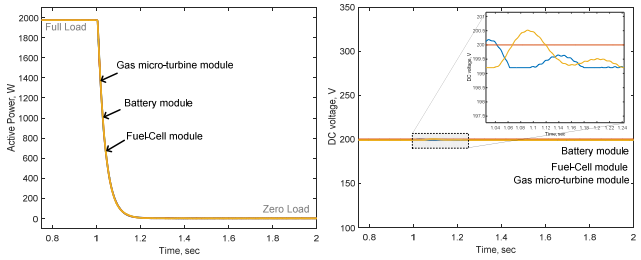

Fig. 5. Detailed simulation results of inverter's power and DC link voltage responses under load change when identical distribution lines are used

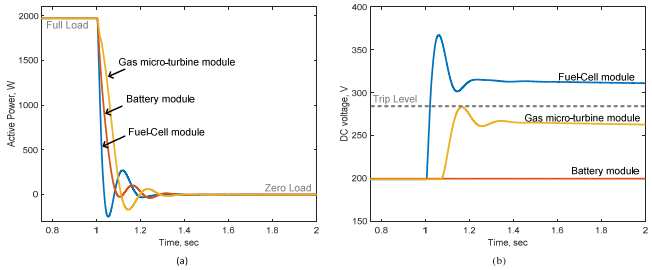

Fig. 6 Detailed simulation results of inverter's power and DC link voltage responses under load change when different distribution lines are used

5. Supplementary Phase Loop Controller

To guarantee stable state responses within a microgrid during the normal operation, Fig. 7 shows two proposed control strategies. Once the DC link voltage exceeds a triggering value, v_{tr}, a supplementary loop is activated. This loop will affect either (a) the frequency or (b) the phase states. In this paper an investigation is carried out to choose the state which has the major influence on the DC link voltage state. This will lead to minimizing the controller effort needed to limit the DC link voltage and thus using a small controller gain, which preserves the stability margins.

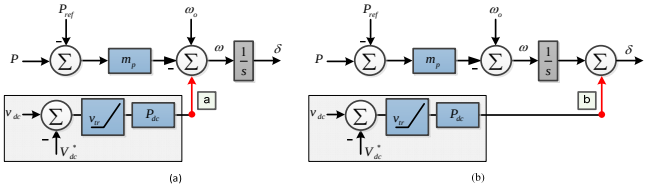

Fig. 7 Proposed controller schemes (a) frequency loop (b) phase loop

By analysing the first control track, (a), where the controller output signal manipulates the frequency state, the small signal output frequency from (1) is derived as:

$$\Delta\omega = -m_p\Delta P + P_d\Delta v_{dc}, \tag{10}$$

where Δv_{dc} is a small signal state of the DC link voltage and derived in [7] as:

$$\Delta v_{dc} = -\frac{k_{dc}}{s}\Delta p_{ins} \tag{11}$$

where k_{dc} is the DC voltage linearizing factor and the negative sign denotes a power negative flow.

By ignoring the power measurement LPF and assuming that the average and instantaneous powers are equal and by substituting (11) in (10) we get

$$\Delta\omega = -(m_p + \frac{P_{dc}k_{dc}}{s})\Delta P \tag{12}$$

Therefore, the phase state is obtained as:

$$\Delta\delta = -\left[\frac{m_p s + P_{dc}k_{dc}}{s^2}\right]\Delta P \tag{13}$$

Similarly, for the control track (b), the frequency and phase states are derived as:

$$\Delta\omega = -(m_p s + P_{dc}k_{dc})\Delta P \tag{14}$$

$$\Delta\delta = -\left[\frac{m_p s + P_{dc}k_{dc}}{s}\right]\Delta P \tag{15}$$

Comparing equations (12) and (14) reveals that method (a) acts as a PI controller for the output power. This might not provide fast action against the imported power. On the other hand, method (b) acts as a PD controller. Here, the power derivative has not been implemented directly but its action has been realized by the proposed loop. It is well-known that the derivative term introduces faster response which is required to limit the imported power and the DC link voltage rise. Furthermore, compared to (15), the additional pole at the origin in (13) adds 90° phase lag which decreases the stability margins. Based on the above discussion, method (b) is expected to perform better.

Table 1 Simulated system parameter

Symbol	Description	Value
$L_{o,i}, R_{o,i}$	Inverter output impedance	1 mH, 0.1Ω
$L_{Line,1}, R_{Line,1}$	Line 1 impedances	1 mH, 0.002Ω
$L_{Line,2}, R_{Line,2}$	Line 2 impedances	2 mH, 0.0035Ω
m_p	Frequency drooping gain	1×10^{-3} rad/s/W
n_q	Voltage drooping gain	1×10^{-3} V/Var
V_o	Voltage set point	110 Vrms
f_o	Frequency set point	50 Hz
ω_c	Measurement filter cut-off frequency	30 rad/sec
V^*_{DClink}	Nominal DC link voltage	200 V
V_{trip}	DC link trip voltage	280 V
v_{tr}	Triggering voltage level	215 V
k_{dc}	Linearization factor relating V^2_{DClink} to V_{DClink}	2.5
C_{dclink}	DC link capacitor for ESS, μGT and PV	$2000\mu F$
P_{dc}	Proposed controller gain	0.5×10^{-3}

6. Participation Factor Analysis

To provide more insight into the superiority of method (b) over method (a), a participation analysis has been carried out [28]. The participation factor, p_{ki} in (16), of states on an eigenvalue is a measure of the influence of the states on that eigenvalue. In contrast, the participation factor, π_{ki} in (17), of eigenvalues on a state is a measure of which mode mostly form the state's response.

$$p_{ki} = r_{ki}l_{ik}, \tag{16}$$

$$\pi_{ki} = \frac{(\mathrm{Re}\{l_{ki}\})^2}{\mathrm{Re}\{l_{ki}\}(\mathrm{Re}\{l_{ki}\})^T}, \quad (17)$$

where k denotes the k^{th} state, i denotes the i^{th} mode l and r denote the left and right eigenvectors.
The system eigenvalues are calculated from (9) as in Table 2 where the dominant eigenvalues are bolded.

Table 2 Microgrid system eigenvalues

Eigenvalue	Location	Eigenvalue	Location
λ_1	0	λ_{14}	**-148+316i**
λ_2	0	λ_{15}	**-148-316i**
λ_3	0	λ_{16}	**-83 +314i**
λ_4	-2147483648+314i	λ_{17}	**-83-314i**
λ_5	-2147483648-314i	λ_{18}	**-5**
λ_6	-2147483648+314i	λ_{19}	**-7**
λ_7	-2147483648-314i	λ_{20}	**-19+6i**
λ_8	-2576255+314i	λ_{21}	**-19-6i**
λ_9	-2576255-314i	λ_{22}	**-22**
λ_{10}	-682516+314i	λ_{23}	**-24**
λ_{11}	-682516-314i	λ_{24}	**-30**
λ_{12}	-30829+314i	λ_{25}	**-30**
λ_{13}	-30829-314i	λ_{26}	0

As the aim is to control the DC link voltage state variable, we will look for the modes which have the major influence on the active power P state variable because P has a direct relationship with the DC link voltage. We can't calculate the participation factors for the DC link voltage state directly as the control loop is still open and the results will be zeros.
Table 3 shows the participation factors of the eigenvalues on the system states. The states of interest are P_1, P_2 *and* P_3.

Table 3 Participation factors of dominant modes on the states

Mode/State	$\Delta\delta_1$	ΔP_1	$\Delta\delta_2$	ΔP_2	$\Delta\delta_3$	ΔP_3
$\lambda_{20,21}$	0.33	0	**0.63**	0	0.04	0
λ_{23}	0.33	0	0.04	0	**0.62**	0
λ_{25}	**1**	0	0	0	0	0

Table 4 Participation factors of the phase/power states on selected modes

	State/ Mode	$\lambda_{14,15}$	$\lambda_{16,17}$	λ_{18}	λ_{19}	$\lambda_{20,21}$	λ_{22}	λ_{23}	λ_{24}	λ_{25}
1	$\Delta\delta_1$	0	0	0	0	0	0	0	0	0
2	ΔP_1	0.003	0	0.08	0.113	0.28	0.16	**0.57**	0.1	**0.43**
3	ΔQ_1	0.007	0	0	0.08	0.12	**0.42**	0.09	**0.4**	0.06
4	Δiod_1	**0.115**	0	0	0	0	0	0	0	0
5	Δioq_1	**0.115**	0	0	0	0	0	0	0	0
6	$\Delta\delta_2$	0.001	0	0.09	**1.23**	**0.54**	0	0.03	0	0
7	ΔP_2	0.000	0	0.01	0.21	**0.53**	0	0.07	0.01	**0.34**
8	ΔQ_2	0.013	0	0	0.15	0.23	0	0.01	**0.4**	0.067
9	Δiod_2	**0.216**	0	0	0	0	0	0	0	0
10	Δioq_2	**0.216**	0	0	0.01	0	0	0	0	0
11	$\Delta\delta_3$	0.000	0	**1.35**	0.085	0.04	0.17	**0.44**	0	0
12	ΔP_3	0	0	0.156	0.016	0.04	0.28	**1.1**	0.1	**0.42**
13	ΔQ_3	0.001	0	0	0.01	0.016	**0.78**	0.17	**0.4**	0.067
14	Δiod_3	0.015	**0.12**	0	0	0	0	0	0	0
15	Δioq_3	0.015	**0.12**	0	0	0	0	0	0	0
16	$\Delta iolineD_1$	**0.115**	0.06	0	0	0	0	0	0	0
17	$\Delta iolineQ_1$	**0.116**	0.06	0	0	0	0	0	0	0
18	$\Delta iolineD_2$	0.031	**0.24**	0	0	0	0.01	0	0	0
19	$\Delta iolineQ_2$	0.031	**0.24**	0	0	0	0.01	0	0	0
20	$\Delta ioloadD_1$	0	0	0	0	0	0	0	0	0
21	$\Delta ioloadQ_1$	0	0	0	0	0	0	0	0	0
22	$\Delta ioloadD_2$	0	0	0	0	0	0	0	0	0
23	$\Delta ioloadQ_2$	0	0	0	0	0	0	0	0	0
24	Δvdc_1	0	0	0	0	0	0	0	0	0
25	Δvdc_2	0	0	0	0	0	0	0	0	0
26	Δvdc_3	0	0	0	0	0	0	0	0	0

Clearly, the eigenvalues $\lambda_{20}, \lambda_{21}, \lambda_{23}$ *and* λ_{25} have the dominant effect on the power responses. Manipulating these modes during transients can reshape the active power responses and hence the DC link voltages can be bounded.

Therefore, another participation factor analysis is carried out to determine which states have the major effect on these modes. Although the frequency is not a direct state from the model, it is an output related to the power state by a scalar as in (5). Therefore, **Table 4** shows the phase and power states participation on the modes of interest as determined earlier. The results show that the phase states have more influence (than the power states) on the modes that will shape the output power and hence the DC link voltage. This confirms the same conclusion drawn from the last section that is method (b) is superior to method (a) and it will lead to smaller controller gain needed to provide the same action.

7. Controller Design

After considering method (b) and by perturbing (1) and calculating the phase state variable, we obtain,

$$\Delta\delta = \frac{\Delta\omega}{s} + P_{dc}\Delta v_{dc} \quad (18)$$

The new phase state equation is calculated as:

$$s\Delta\delta = -m_p\Delta P - P_{dc}k_{dc}\Delta p_{ins}. \quad (19)$$

Equation (19) has been incorporated into the system state space matrix in (9), where the ΔP *and* Δp_{ins} are redefined, instead of the original phase state equation [23]. Fig. 8 shows the eigenvalues when the proposed controller gain changes as $1 \times 10^{-4} > P_{dc} > 2 \times 10^{-3}$. From the figure we can observe the following:

- Increasing the proposed controller gain P_{dc} influences the targeted eigenvalues $\lambda_{20,21}$ *and* λ_{23}, which is in agreement with **Table 5**. However, some other eigenvalues are also influenced such as $\lambda_{14,15}$ *and* $\lambda_{16,17}$ because of the coupling between the state variables and eigenvalues, which can't be easily analysed. Also, the targeted λ_{25} has a negligible change as it is mainly subject to the measuring filter bandwidth. $\lambda_{18}, \lambda_{19}$ *and* λ_{24}, are not affected.
- The increment of P_{dc} moves the targeted eigenvalues far away to the left thus increasing the system damping. However, high frequency eigenvalues also move toward the imaginary axis and at some high gains the system will become unstable.

The red circles denote the eigenvalues of the system when $P_{dc} = 0.5 \times 10^{-3}$, where the non-oscillatory eigenvalues are dominant.

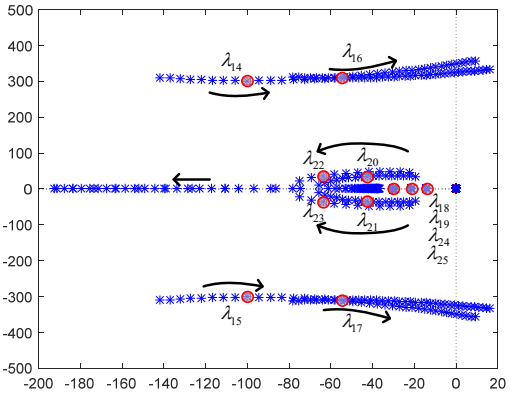

Fig. 8 Root locus of the system when $1 \times 10^{-4} > P_{dc} > 2 \times 10^{-3}$

8. Simulation Results

A microgrid consisting of three inverters as shown in Fig. was simulated in Matlab/SimPowerSystem to validate the performance of the proposed control scheme. The converters and inverters are represented by the ideal source models. The simulation parameters are listed in **Table 1**. The three inverters were supplying the full load of 2kW each (local load is 6kW), and at t= 1 s the load was disconnected. The power responses are shown in Fig. 9a. It is clear that the response is well-damped thanks to the proposed controller which is activated automatically when the DC voltage exceeds v_{tr}. It is worth comparing this with the results in Fig. 6 which is for the same system but without the controller been activated. In addition, the DC link voltages in Fig. 9b are bounded and they are below the trip level, which confirms the effectiveness of the proposed strategy. Although, the average power responses in Fig. 9a did not show any reverse flow, the instantaneous power of the Fuel cell has in fact a reverse power and that is shown in Fig. 10. This reverse power flow caused the DC link capacitor to charge.

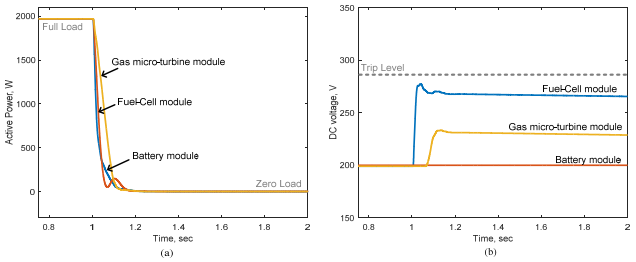

Fig. 9 Under load change, (a) averaged active power response and (b) DC link voltages

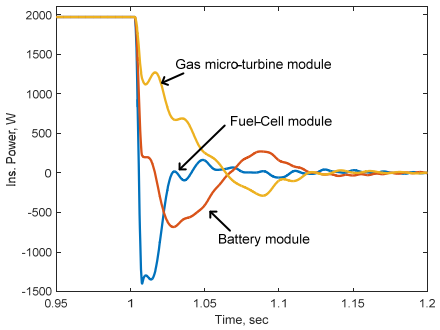

Fig. 10 Instantaneous power flow between the inverters

Fig. 11 shows the averaged active power and the DC voltage responses when the proposed controller's gain is $P_{dc} = 1 \times 10^{-3}$. The system is unstable and the oscillating frequency is found to be 314 rad/ sec and this agrees with the prediction from Fig. 8 where the system becomes unstable and the oscillation frequency is 312 rad/sec.

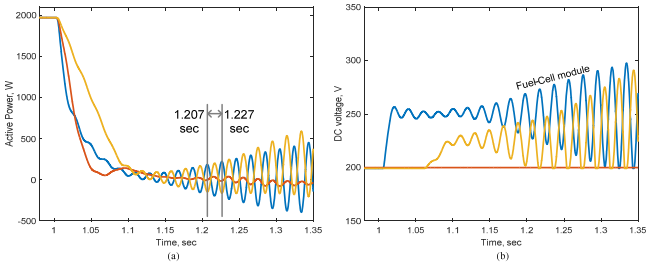

Fig. 11 Averaged power (a) and DC link voltage (b) responses when $P_{dc} = 1 \times 10^{-3}$

To confirm the findings of the analytical approach with regards to the superiority of method (b) over method (a), Fig. 12 shows the responses when the control loop (a) is adopted with $P_{dc} = 5 \times 10^{-3}$. The gain has been chosen to give the same ability to limit the DC link voltage as shown in Fig. 9b. It is obvious that the gain is higher than the one used in method (b), which confirms that the method (b) needs less effort to limit the DC voltage. Furthermore, the responses of power and DC link voltage are very oscillatory compared to that in Fig. 9.

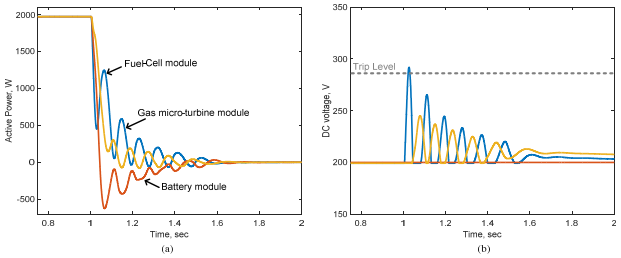

Fig. 12 Averaged power (a) and DC link voltage (b) responses when method (a) is used

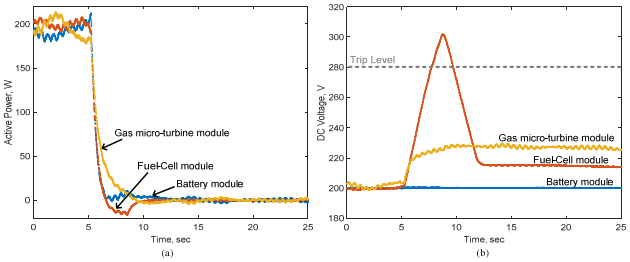

Fig. 13 Experimental averaged power (a) and DC link voltage (b) responses under load dropping

9. Experimental Results

A single phase microgrid consisting of three DC/AC inverters and three DC/DC converters as shown in Fig.1 has been built in the lab. The energy sources are lead-acid battery bank and two fixed DC power sources representing unidirectional energy source. One of the DC/DC converters has been configured as a bidirectional converter to interface the battery while the others were configured as unidirectional boost converters. The control algorithms have been realized using OPAL-RT real time simulator. The parameters of the system and controllers are shown in **Table 5**. Fig. 13 shows the active power responses and the DC link voltages of the three inverters when the power of each was 200W (total load was 600W). At t = 5 sec the load was disconnected. During the transients the circulating power between the inverters charged the fuel cell and micro turbine DC link capacitors. The DC voltage of the fuel cell module exceeded the trip level causing a shutdown of the inverter. The proposed controllers using methods (a) and (b) were implemented experimentally to validate the theoretical and simulation results. Both Fig. 14 and Fig. 15 show the averaged active power and the DC link voltage responses during the load changes from 200W to zero when using method (a) and method (b), respectively, for different controller gains values. Obviously, increasing the controller gain, $P_{dc} = [0.5,1,5] \times 10^{-3}$, in both methods provides faster responses and better performance in limiting the rise of the DC link voltage. However, method (b) in Fig. 15 produces a smoother and highly damped response when it is compared with method (a) in Fig. 14, which has oscillatory responses. This confirms the findings in the previous sections. The oscillatory response in Fig. 14 indicates that the dominant eigenvalues of the system are close to the

imaginary axis with higher frequency. For all gain values, method (b) is superior and can provide more reliable and satisfactory responses. The size of the DC link capacitor can influence the DC link voltage transient as discussed in [7]. Therefore, larger capacitor can delay the trip action but still the proposed controller is needed to cease the circulating energy.

Again, choosing high droop gain might equip the inverter with a fast response mitigating the circulating current. However, in some cases, this choice is limited because of:

- droop control loop bandwidth should be less than the inner loops,
- high droop gains produce oscillations and impact the stability, and
- high output power inverters require low droop gains to be within the allowable frequency variations.

The proposed controller approved its performance in such cases as a supplementary loop for the traditional droop control and to avoid selecting high gains.

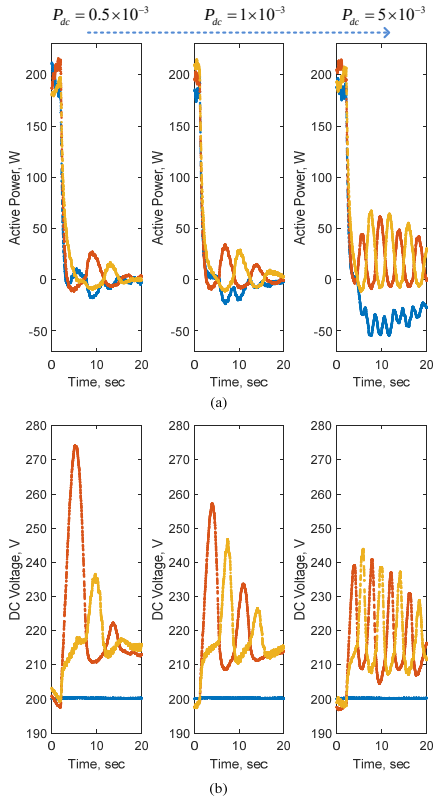

Fig. 14 Experimental results when method (a) is used

10. Conclusion

This paper has investigated the performance of parallel inverters serving within an islanded microgrid. The study emphasized that, similar droop gains can't guarantee identical power responses during transient in all cases. If a significant line impedance mismatch is existing, the circulating transient power might by sufficient to degrade the stability. It is found that the proposed phase supplementary loop performs more effectively than the frequency loop in stabilizing the microgrid DC link voltage states. It is worth mentioning that this loop will be activated temporarily during the transient if the DC voltage exceeded a threshold. The steady state error appears just in case of zero load transition. However, it is not a big concern as once a load is connected again, it is enough to discharge this excess energy and to retain a zero error. The theoretical analysis and the performance of the proposed controller have been validated by simulation and experimental results.

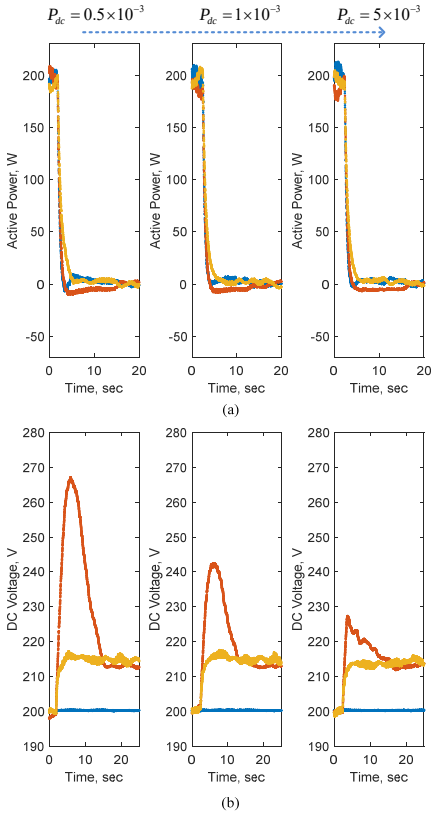

Fig. 15 Experimental results when method (b) is used

Table 5 Experimental setup parameters

Inverters parameters		DC/DC Converters	
L_1	$4mH$	L_{DC}	$0.8mH$
C	$25\mu F$	V_{bat}	125V
L_2	$2mH$	V_{dc}	$200\,V$
V	$110\,V$	DC/DC current controller	
ω	$2\pi.50\,rad/s$	k_{p_c}	5×10^{-3}
C_{dc}	$1100\mu F$	k_{i_c}	1
L_{line1}	$1mH$	DC/DC voltage controller	
L_{Line2}	$2mH$	k_{p_v}	20
f_{sw}	$10kHz$	k_{i_v}	50
Inverter voltage controller		Proposed controller	
k_v	0.01	P_{dc}	0.5×10^{-3}
k_c	3	v_{tr}	$215\,V$
L_v	$8mH$	v_{trip}	$280\,V$
Droop controller			
m_p	1×10^{-3}		
n_q	1×10^{-3}		
ω_c	$2\,rad/s$		

11. References

1. 'Ieee Standard for Interconnecting Distributed Resources with Electric Power Systems, Ieee Standard 1547, P. 16.', 2003.

2. Issa, W., Sharkh, S., Mallick, T., and Abusara, M., 'Improved Reactive Power Sharing for Parallel-Operated Inverters in Islanded Microgrids', *Journal of Power Electronics*, 2016, 16, (3), pp. 1152-1162.

3. Coelho, E.A., Wu, D., Guerrero, J.M., Vasquez, J.C., Dragicevic, T., Stefanovic, C., and Popovski, P., 'Small-Signal Analysis of the Microgrid Secondary Control Considering a

Communication Time Delay', *IEEE TRANSACTIONS ON INDUSTRIAL ELECTRONICS*, 2016, PP, (99), pp. 1-1.
4. Zhong, Q.C. and Zeng, Y., 'Universal Droop Control of Inverters with Different Types of Output Impedance', *IEEE Access*, 2016, 4, pp. 702-712.
5. Issa, W.R., Khateb, A.H.E., Abusara, M.A., and Mallick, T.K., 'Control Strategy for Uninterrupted Microgrid Mode Transfer During Unintentional Islanding Scenarios', *IEEE TRANSACTIONS ON INDUSTRIAL ELECTRONICS*, 2017, PP, (99), pp. 1-1.
6. Avelar, H.J., Parreira, W.A., Vieira, J.B., de Freitas, L.C.G., and Coelho, E.A.A., 'A State Equation Model of a Single-Phase Grid-Connected Inverter Using a Droop Control Scheme with Extra Phase Shift Control Action', *IEEE Transactions on Industrial Electronics*, 2012, 59, (3), pp. 1527-1537.
7. Issa, W., Abusara, M., and Sharkh, S., 'Control of Transient Power During Unintentional Islanding of Microgrids', *IEEE Transactions on Power Electronics*, 2014, 30, (8), pp. 4573 - 4584.
8. Guerrero, J.M., De Vicuna, L.G., Matas, J., Castilla, M., and Miret, J., 'A Wireless Controller to Enhance Dynamic Performance of Parallel Inverters in Distributed Generation Systems', *IEEE TRANSACTIONS ON POWER ELECTRONICS*, 2004, 19, (5), pp. 1205-1213.
9. Ritwik Majumder, B.C., Arindam Ghosh,Rajat Majumder, Gerard Ledwich and Firuz Zare, 'Improvement of Stability and Load Sharing in an Autonomous Microgrid Using Supplementary Droop Control Loop', *IEEE Transactions on Power Systems*, 2010, 25, (2).
10. Chen, Y.M., Liu, Y.C., Hung, S.C., and Cheng, C.S., 'Multi-Input Inverter for Grid-Connected Hybrid Pv/Wind Power System', *IEEE TRANSACTIONS ON POWER ELECTRONICS*, 2007, 22, (3), pp. 1070-1077.
11. A. P. Sakis Meliopoulos, G.J.C., 'Small Signal Stability Analysis of the Integrated Power System - Microgrid Model', in, *Bulk Power System Dynamics and Control*, (2004)
12. Vasquez, J.C., Guerrero, J.M., Luna, A., Rodríguez, P., and Teodorescu, R., 'Adaptive Droop Control Applied to Voltage-Source Inverters Operating in Grid-Connected and Islanded Modes', *IEEE Transactions on Industrial Electronics*, 2009, 56, (10), pp. 4088-4096.
13. Escobar, G., Mattavelli, P., Stankovic, A.M., Valdez, A.A., and Leyva-Ramos, J., 'An Adaptive Control for Ups to Compensate Unbalance and Harmonic Distortion Using a Combined Capacitor/Load Current Sensing', *IEEE TRANSACTIONS ON INDUSTRIAL ELECTRONICS*, 2007, 54, (2), pp. 839-847.
14. Zhang, C., Guerrero, J.M., Vasquez, J.C., and Coelho, E.A.A., 'Control Architecture for Parallel-Connected Inverters in Uninterruptible Power Systems', *IEEE TRANSACTIONS ON POWER ELECTRONICS*, 2016, 31, (7), pp. 5176-5188.
15. Tan, K.T., So, P.L., Chu, Y.C., and Chen, M.Z.Q., 'Coordinated Control and Energy Management of Distributed Generation Inverters in a Microgrid', *IEEE TRANSACTIONS ON POWER DELIVERY*, 2013, 28, (2), pp. 704-713.
16. Moghadasi, A., Sargolzaei, A., Khalilnejad, A., Moghaddami, M., and Sarwat, A., 'Model Predictive Power Control Approach for Three-Phase Single-Stage Grid-Tied Pv Module-Integrated Converter', in, *2016 IEEE Industry Applications Society Annual Meeting*, (2016)
17. JUAN C. VASQUEZ, J.M.G., JAUME MIRET, MIGUEL CASTILLA, and LUIS GARCI´A DE VICUN˜ A, Hierarchical Control of Intelligent Microgrids', *IEEE INDUSTRIAL ELECTRONICS MAGAZINE*, (2010)
18. Mahmood, H., Michaelson, D., and Jin, J., 'Control Strategy for a Standalone Pv/Battery Hybrid System', in, *38th Annual Conference on IEEE Industrial Electronics Society -IECON 2012* (2012)
19. Al Badwawi, R., Issa, W., Mallick, T., and Abusara, M., Power Management of Ac Islanded Microgrids Using Fuzzy Logic', *8th IET International Conference on Power Electronics, Machines and Drives (PEMD)*, (2016)
20. Kolli, A., Gaillard, A., De Bernardinis, A., Bethoux, O., Hissel, D., and Khatir, Z., 'A Review on Dc/Dc Converter Architectures for Power Fuel Cell Applications', *Energy Conversion and Management*, 2015, 105, pp. 716-730.
21. Mane, S., Kadam, P., Lahoti, G., Kazi, F., and Singh, N.M., 'Optimal Load Balancing Strategy for Hybrid Energy Management System in Dc Microgrid with Pv, Fuel Cell and Battery Storage', in, *2016 IEEE International Conference on Renewable Energy Research and Applications (ICRERA)*, (2016)
22. Ziaeinejad, S., Sangsefidi, Y., and Mehrizi-Sani, A., 'Fuel Cell-Based Auxiliary Power Unit: Ems, Sizing, and Current Estimator-Based Controller', *IEEE Transactions on Vehicular Technology*, 2016, 65, (6), pp. 4826-4835.
23. Issa, W., Abusara, M., Sharkh, S., and Tapas, M., 'A Small Signal Model of an Inverter-Based Microgrid Including Dc Link Voltages', in, *17th European Conference on Power Electronics and Applications*, (EPE 2015, 2015)
24. Pogaku, N., Prodanovic, M., and Green, T.C., 'Modeling, Analysis and Testing of Autonomous Operation of an Inverter-Based Microgrid', *IEEE TRANSACTIONS ON POWER ELECTRONICS*, 2007, 22, (2), pp. 613-625.
25. Rasheduzzaman, M., Mueller, J., and Kimball, J., 'An Accurate Small-Signal Model of Inverter-Dominated Islanded Microgrids Using Dq Reference Frame', *IEEE Journal of Emerging and Selected Topics in Power Electronics*, 2014.
26. Abusara, M.A., Sharkh, S.M., and Guerrero, J.M., 'Improved Droop Control Strategy for Grid-Connected Inverters', *Sustainable Energy, Grids and Networks*, 2015, 1, pp. 10-19.
27. Josep M. Guerrero, L.G.d.V., José Matas, Miguel Castilla and Jaume Miret, 'Output Impedance Design of Parallel-Connected Ups Inverters with Wireless Load-Sharing Control', *IEEE TRANSACTIONS ON INDUSTRIAL ELECTRONICS*, 2005, 52, (4).
28. Zhang, C., Coelho, E.A.A., Guerrero, J.M., and Vasquez, J.C., 'Modular Online Uninterruptible Power System Plug N Play Control and Stability Analysis', *IEEE TRANSACTIONS ON INDUSTRIAL ELECTRONICS*, 2016, 63, (6), pp. 3765-3776.